DRAFT VERSION MARCH 8, 2009
Preprint typeset using LaTeX style emulateapj v. 12/14/05

Chandra DISCOVERY OF AN INTERMEDIATE POLAR IN BAADE'S WINDOW

JAESUB HONG[1*], MAUREEN VAN DEN BERG[1], JONATHAN E. GRINDLAY[1], SILAS LAYCOCK[2], AND PING ZHAO[1]

Draft version March 8, 2009

ABSTRACT

We have discovered an intermediate polar (IP) in the 100 ks *Chandra* observation of Baade's Window (BW), a low extinction region at about 4° south of the Galactic Center. The source exhibits large X-ray modulations at a period of 1028.4 s in the 0.3 – 8 keV band. The X-ray spectral fit with a power law model shows the integrated spectrum is intrinsically hard (photon index, $\Gamma = 0.44 \pm 0.05$) and moderately absorbed ($N_{\rm H} = 1.5 \pm 1.0 \times 10^{21}$ cm^{-2}). The relatively poor statistics only allows for a mild constraint on the presence of an iron emission line (equivalent width = 0.5 ± 0.3 keV at 6.7 keV). Quantile analysis reveals that the modulations in the X-ray flux strongly correlate with spectral changes that are dominated by varying internal absorption. The X-ray spectrum of the source is heavily absorbed ($N_{\rm H} > 10^{22}$ cm^{-2}) during the faint phases, while the absorption is consistent with the field value ($\sim 10^{21}$ cm^{-2}) during the bright phases. These X-ray properties are typical signatures of IPs. Images taken with the IMACS camera on the Magellan 6.5m telescope show a faint ($V \sim 22$), relatively blue object ($B_0 - V_0 \gtrsim 0.05$) within the 2σ error circle of the *Chandra* source, which is a good candidate for being the optical counterpart. If we assume a nominal range of absolute V magnitude for a cataclysmic variable ($M_V \sim 5.5 - 10.5$) and the known reddening in the region ($A_V = 1.4$ at > 3 kpc), the source would likely be at a distance of 2–10 kpc and not in the local solar neighborhood. The corresponding average X-ray luminosity would be $6 \times 10^{31} - 10^{33}$ ergs s^{-1} in the 2–8 keV band. Assuming the space density of IPs follows the stellar distribution, which is highly concentrated in the Galactic Bulge, the source is probably a bright IP belonging to the Galactic Bulge X-ray population, the majority of which is now believed to be magnetic cataclysmic variables.

Subject headings: Galaxy: bulge — X-ray: binaries — cataclysmic variables

1. INTRODUCTION

Intermediate Polars (IPs) are a type of magnetic cataclysmic variable (CV), where the magnetic field of the accretor, a white dwarf (WD), disrupts the inner portion of the accretion disk and channels the accretion flow into the magnetic poles of the WD (Patterson 1998). As the WD spins, this channeling gives rise to a pulsation, a tell sign of an IP, which is typically found in the period range of $\sim 100 - 1000$s s. The magnetic field on the surface of the WD in IPs is typically about 10^{6-7}G, and the ratio of the spin to orbital period of IPs is found in a wide range from 0.01 to <1. Some IPs are on the evolutionary path to their cousins, the polars, where the orbital and WD spin periods are usually locked under the strong magnetic fields that convert the whole accretion flow into a stream (Norton, Wynn & Somerscales 2004). Magnetic CVs provide unique astrophysical laboratories for studying physics in extreme conditions, stellar and binary evolution, which is important to make a census of Galactic population and understand their evolution. There are about 33 confirmed and 72 candidate IPs today, and the full catalogue is found in Ritter & Kolb (2003)[3].

The 72 IP candidates contain seven periodic X-ray sources at the Galactic Center (GC), which are part of ~ 2300 X-ray sources discovered in the deep *Chandra* observations of the Sgr A* field (Muno et al. 2003a). The exact nature of the majority of the GC X-ray population still remains elusive: direct identification at other wavelength is difficult due to high obscuration by dust and source confusion due to high star density. Therefore, the discovery of these IP candidates is particularly interesting since it supports the idea of magnetic CVs as the leading candidates for the majority of the GC X-ray sources (Muno et al. 2004; Laycock et al. 2005). If true, this also implies the GC X-ray population is very old.

In order to explore the X-ray population in the Galactic Bulge (GB) without obscuration by the intervening dust, we have observed three low extinction Windows within 4° of the GC with the *Chandra* X-ray observatory (van den Berg et al. 2006, 2009; Hong et al. 2009). The initial population study on the X-ray sources in these Windows and four GB fields has revealed that the GB X-ray sources extend out to $> 1.4°$ from the GC with a projected source density that follows a $1/\theta$ relation, where θ is the angular offset from the GC (Hong et al. 2009). In addition, the similarity of the X-ray spectra of the hard X-ray sources in these fields – an intrinsically hard continuum with the presence of an iron emission line – indicates a single class of sources, likely magnetic CVs, could make up both the GC and GB X-ray populations.

As part of our efforts to identify the nature of these sources, we have searched for periodic modulations in the X-ray emission of the bright X-ray sources (net counts ≥ 250 in the 0.3–8 keV range) in the Window fields using the Lomb-Scargle algorithm (Scargle 1982). As a result, we have discovered an IP in Baade's Window (BW) based on a strong pulsation correlated with the X-ray spectral variation (§2). We explore the properties of this X-ray source (§3) and the potential optical counterpart (§4) that lead to its identification as an IP. We discuss the possibility that the system belongs to the GB X-ray population (§5).

2. OBSERVATION AND TIMING ANALYSIS

* Send requests to J. Hong at jaesub@head.cfa.harvard.edu
[1] Harvard-Smithsonian Center for Astrophysics, 60 Garden St., Cambridge, MA 02138
[2] Gemini Observatory, 670 N. A'ohoku Place, Hilo, HI 96720
[3] See the on-line catalogue at http://physics.open.ac.uk/RKcat/ and http://asd.gsfc.nasa.gov/Koji.Mukai/iphome/iphome.html for the latest update.

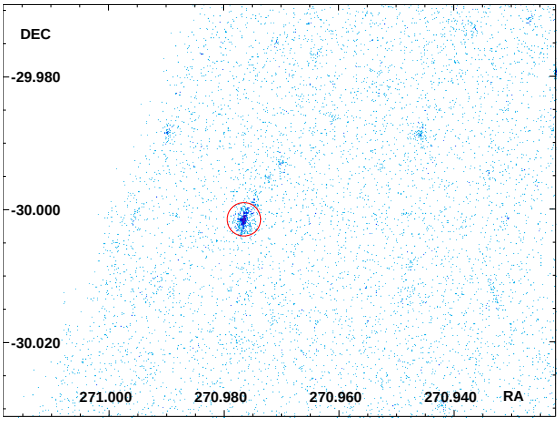

FIG. 1.— The raw X-ray sky image around CXOPS J180354.3-300005. The (red) circle indicates the source region used for the aperture photometry. The morphology of the event distribution is consistent with the expected point spread function at the source location.

We have observed BW on 2003 July 9 (Obs. ID 3780), Stanek's Window (SW) on 2004 February 14/15 (Obs. ID 4547 and 5303), and Limiting Window (LW) on 2005 August 19/22 and October 25 (Obs. ID 5934, 6362 and 6365) with the *Chandra* ACIS-I instrument (van den Berg et al. 2006, 2009; Hong et al. 2009). The data were analyzed as a part of our survey program, the *Chandra* Multi-wavelength Plane (ChaMPlane) survey, which is designed to constrain the Galactic population of low luminosity accretion sources, CVs in particular (Grindlay et al. 2005). In summary, we search for X-ray point sources using a wavelet algorithm (*wavdetect*, Freeman et al. 2002) and perform aperture photometry to extract the basic X-ray properties. The details of the analysis procedures are described in Hong et al. (2005, 2009).

In order to find periodic X-ray modulations in the light curves of these X-ray sources, we have performed a Lomb-Scargle periodicity search on the bright X-ray sources (net counts ≥ 250 in 0.3–8.0 keV) discovered in the 100 ks observation of the Window fields - BW (Obs. ID 3780), Stanek Window (Obs. ID 4547 and 5303) and Limiting Window (Obs. ID 5934, 6362 and 6365) (Hong et al. 2009). The events are selected by the good time intervals (GTIs), where the background fluctuation is less than 3σ above the mean level (Hong et al. 2005). The arrival time of each photon is bary-center corrected using the CIAO tool `axbary`[4]. For each source, we generate the light curves in time bins of four multiples (1, 4, 8 and 16) of the CCD integration time (3.2 s). Then we apply the Lomb-Scargle algorithm and calculate the power spectrum for the light curves at all four time resolutions.

We have found that one source in BW, CXOPS J180354.3-300005 exhibits a clear sign of a periodic modulation with greater than 99% of the confidence level (CL). The source was detected with 510 ± 24 net counts in the broad band (B_X, 0.3–8 keV) after background subtraction. Fig. 1 shows the raw sky image around the source marked by the (red) circle of the 95% point spread function (PSF). The source only appears to be extended due to the large offset (8.5′) from the aimpoint of the instrument, but a simulated PSF by a CIAO tool `mkpsf` at the source position closely resembles the event distribution of the source, indicating that the source is consistent with a point source.

[4] http://cxc.harvard.edu

Fig. 2a shows the power spectrum of the source in the frequency domain along with horizontal lines indicating 90, 95 and 99% CLs. This power spectrum is based on the light curve at the 12.8 s time resolution and the results based on the other three time resolutions are very similar. The power spectrum indicates the source exhibits pulsations at a period of 1028.4 $\pm$ 3.8 s. The error of the period estimate is the 1σ equivalent spread of the peak in the power spectrum, which is calculated by a fit to the peak with a Gaussian function in the period domain. The observed period is somewhat close to a possible spurious period (1000 s). Sources falling near the edges or node boundaries of the chips can exhibit spurious modulations at a period of 707 or 1000 s (or their harmonics) due to the dither motion of the *Chandra* X-ray observatory. However, we consider the periodic modulation found in CXOPS J180354.3-300005 to be real because first, the source is not near the chip edges or the node boundaries and second, the X-ray spectral properties of the source strongly correlate with the flux modulation as demonstrated below.

Fig. 2b shows the folded light curves at the pulsation period in the soft (0.3–2.0 keV), hard (2.0–8.0 keV) and broad (0.3–8.0 keV) bands. The folded light curve of the broad band is shifted up by 1 cts ks^{-1} for clarity. The smooth lines are calculated using the LOWESS algorithm (Cleveland 1994) and color-coded by the phase for a later reference in the spectral analysis (§3). The data points are calculated at the 10 equal-sized phase bins of width 0.1. The net count per bin ranges from $\sim$ 18 to 90 in the 0.3–8.0 keV range.

We define the modulation depth as $(R_{\rm max} - R_{\rm min})/(R_{\rm max} + R_{\rm min})$ where $R_{\rm max}$ and $R_{\rm min}$ are the maximum and minimum of the fitted amplitudes respectively. Using a fit to the 10 data points with a sinusoidal function, we estimate the modulation depth is (90 ± 10)%, (42 ± 10)% and (53 ± 8)% for the soft, hard, and broad bands respectively. The modulation amplitude varies with the energy band, which we will explore in more detail using quantile analysis in §3.

BW was also observed with the EPIC cameras on the *XMM-Newton* observatory in two separate pointings with $\sim$ 20–25 ks exposure each on 2002 March 11 and 2004 September 30. The data from both observations are publicly available. Our source was detected as 2XMM J180354.3-300004[5] at large offsets (5.7′ and 7.6′) from the aimpoint in both observations. Unfortunately, in the four datasets out of six total (three cameras and two pointings), the source fell near a chip gap. In both PN observations, which would have provided an interesting result because of the superior sensitivity at high energies than the *Chandra* ACIS instruments, the central part of the PSF overlapped with a chip gap, rendering the data practically unusable. Three MOS observations (including one with the source marginally close ($\sim$30″) to the chip edge) appear to produce relatively *clean* dataset of the source, but the poor statistics (net counts: $\sim 60-80$ each in 0.3–8 keV) did not allow for any significant detection of pulsation. Therefore, in the following, we mainly consider the *Chandra* data for the X-ray observation of the source.

3. X-RAY SPECTRUM AND VARIATION

Table 1 summarizes the results of the spectral model fits to the integrated X-ray spectrum of the source using a power law model with and without an iron emission line at 6.7 keV. The Fe He-α XXV line is considered because many of the GC X-ray sources exhibit this line more prominently than the neu-

[5] http://xmm.esac.esa.int/xsa/

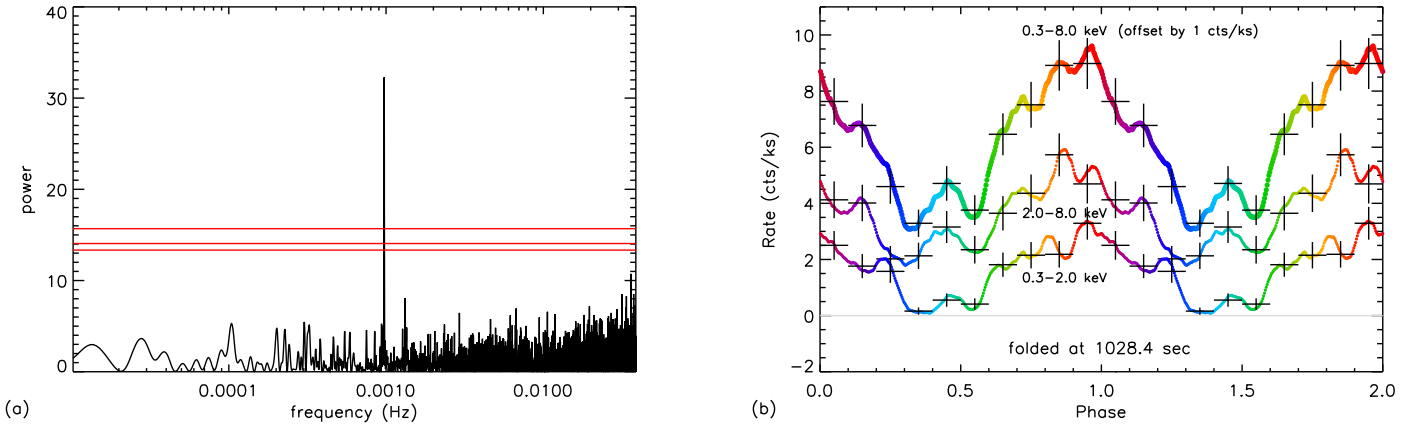

FIG. 2.— The power spectrum (a) of CXOPS J180354.3-300005 in the broad band (0.3–8.0 keV) and the folded light curves (b) in the soft (0.3–2.0 keV), hard (2.0–8.0 keV), and broad bands (phase = 0 at JD 2452830.0). The primary modulation is found at $9.727 \pm 0.036 \times 10^{-4}$ Hz or 1028.4 ± 3.8 s. The horizontal lines in (a) represent the confidence levels (CLs) of 90, 95 and 99%. The smooth lines in (b) are generated by the LOWESS alghorithm and color-coded by the phase for a later reference (Fig. 4). The data points are calculated in the equal phase bins (0.1). The modulation depth is estimated to be (90 ± 10)%, (42 ± 10)% and (53 ± 8)% for the soft, hard, and broad bands respectively. The folded light curves in the broad band are shifted up by 1 cts ks^{-1} for clarity.

TABLE 1
SPECTRAL MODEL FITS AND QUANTILE ANALYSIS OF THE INTEGRATED X-RAY SPECTRUM OF CXOPS J180354.3-300005

Model	Spectral Fits				Quantile Analysis			Flux	
	N_{H22} ($\times 10^{22}$cm^{-2})	Γ	EW (keV)	χ^2/DoF	N_{H22} ($\times 10^{22}$cm^{-2})	Γ	EW (keV)	0.5 – 2 keV ($\times 10^{-13}$ ergs cm^{-2} s^{-1})	2 – 8 keV ($\times 10^{-13}$ ergs cm^{-2} s^{-1})
Chandra									
PL	0.15(10)	0.44(5)	-	12.6/22	0.28(21)	0.49(18)	-	0.13(1)	1.20(7)
PL+Fe	0.22(10)	0.53(5)	0.5(3)	10.3/20	0.39(22)	0.63(18)	0.5	0.14(1)	1.19(7)
XMM-Newton MOS									
PL					$0.61^{+0.64}_{-0.41}$	$0.60^{+0.41}_{-0.39}$	-	0.19(12)	1.25(43)

For the *Chandra* data, the flux estimates are based on the spectral model fits. The errors are of statistical origin, based on the photon counts using small-number statistics by Gehrels et al. (1986). The PL+Fe model in quantile analysis assumes a 0.5 keV EW for the iron line at 6.7 keV. In the *XMM-Newton* data, we combine three datasets and use quantile analysys under a simple power law. The datasets comprise the MOS1 observation in the 2002 pointing, and both the MOS1 & MOS2 observations in 2004. The flux estimate is based on the quantile analysis of the combined dataset, and the errors are the quadratic sum of the statistical error and the standard deviation of the three datasets. DoF stands for degrees of freedom.

tral Fe line at 6.4 keV (Wang et al. 2002; Muno et al. 2003; Hong et al. 2009). Both models produce acceptable fits, and the spectrum is intrinsically hard ($\Gamma \sim 0.4$) and moderately absorbed ($N_{\rm H22} \sim 0.2$). Fig. 3 shows the spectral model fit to the integrated spectrum of the source using the power law plus the iron line. There is a hint of an emission line in the 6 – 7 keV energy range in the spectrum but the poor statistics does not provide a significant constraint on the presence of the iron line. The estimated equivalent width (EW) of the iron line at 6.7 keV is 0.5 ± 0.3 keV. In the case of the thermal Bremsstrahlung or thermal plasma model, the model temperatures are not well constrained because the resulting values are too high (kT$>$ 20 keV) for the given energy range (0.3–8 keV) of the spectrum.

The total column density in the direction of CXOPS J180354.3-300005 is estimated to be $N_{\rm H22} = 0.25(8)$ by Marshall et al. (2006) or 0.25(5) by Sumi (2004), using $N_{\rm H22} = 0.179\ A_V$ (Predehl & Schmitt 1995). The former estimates are given in a set of distances starting from 2.75 kpc for the BW field and the latter estimates are given at a finer angular resolution ($\sim 0.5' - 2.0'$) than the former ($\sim 8.0'$). There are also other estimates for the extinction in the BW such as $\sim$ 0.34 by Schlegel et al. (1998) or $\sim$ 0.41 by Drimmel et al. (2003), but the underlying models of these estimates are not accurate in this region.

In order to explore the spectral variation as a function of the modulation phase, we use quantile analysis. Quantile analysis is a bias-free spectral classification method, suitable for faint sources or for investigating subsets of the data that do not allow for spectral model fits due to low statistics (Hong et al. 2004). We calculate the quantile values of the X-ray spectra of the source as a function of modulation phase using a sliding phase window of a fixed size (0.1). Fig. 4 shows such a quantile diagram[6], which is overlaid with power law and thermal Bremsstrahlung model grids for easy interpretation. The energy quantile E_x corresponds to the energy below which x% of the counts are detected in the 0.3–8.0 keV range.

The filled circles are color-coded to match the phase of the smooth line in the folded light curve in Fig. 3b for easy comparison and the data points with the error bars are from the same 10 data points in the folded light curve. Table 1 also shows the spectral parameters estimated by quantile analysis of the integrated spectrum (marked by a hollow cross in Fig. 4) and the results are consistent with the spectral fit.

The quantile diagram reveals dramatic spectral changes as a function of pulsation phase, illustrated by a large loop formed counter-clockwise as the X-ray flux modulates in a full cycle (see the track in Fig. 4b). The spectral variation is expected from the energy dependence of the modulation depth seen in Fig. 2. In the quantile diagram, we can also see that the spectral changes are dominated by varying extinction. During the bright phases, the spectrum is relatively unabsorbed with $N_{\rm H22} \lesssim 1$, less than or consistent with the field extinction (e.g. the yellow and red points in Fig. 2b & 4b), but during the faint phases, especially around phases 0.3 – 0.6 (e.g. the light blue points), the spectrum is heavily absorbed with $N_{\rm H22} > 5$. Since the field extinction is very low, the additional increase in extinction must be intrinsic to the source. Note the long axis of the data loop in the quantile diagram is largely parallel to the direction related to changes in absorption for both spectral models as shown in Fig. 4. In fact, this is true in general regardless of the specral models.

[6] Note the definition of the x-axis in this quantile diagram is different from the one suggested by Hong et al. (2004). The new definition is $\log_{10}(E_{50}/E_{\rm lo})/\log_{10}(E_{\rm hi}/E_{\rm lo})$ in general, where $E_{\rm lo}$ and $E_{\rm hi}$ are the lower and upper bound of the energy range respectively. We believe the new definition is more reflective of the instrument response and the confined range (0–1) allows for statistically more uniform response throughout the phase space of quantile diagram (Hong et al. 2009b).

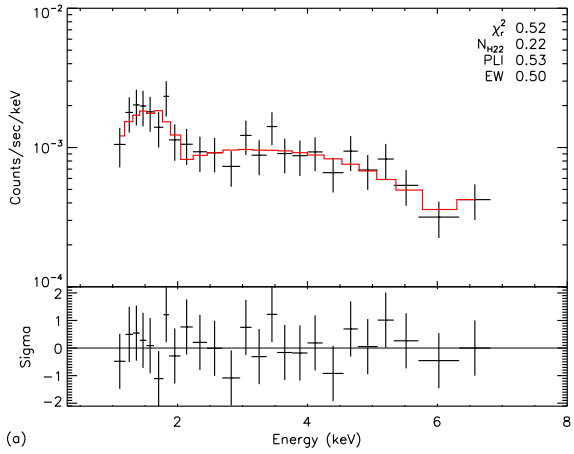

FIG. 3.— The spectral model fit to the integrated X-ray spectrum of CXOPS J180354.3-300005 under a power law plus an iron line at 6.7 keV. See also Table 1. The spectral fit shows a hint of the iron emission line.

Table 1 also shows the results of the *XMM-Newton* data for comparison, for which we combine three relatively clean datasets (the MOS1 observation in 2002, both MOS1 and MOS2 in 2004). The overall spectral properties and the flux estimates of the *XMM-Newton* data based on the quantile analysis are consistent with those derived from the *Chandra* data.

4. OPTICAL COUNTERPART

On 2007 May 8, we observed the three Window fields with the Inamori Magellan Areal Camera and Spectrograph (IMACS) on the 6.5 m Magellan (Baade) telescope at Las Campanas, Chile. Under good conditions (seeing FWHM $\sim 0.5''$, clear sky) we obtained a dithered set of 5 pointings in the f/4 configuration ($15'$ field, $0.2''$/pixel) to cover an $18' \times 18'$ region of BW. This provided a total exposure time of 500 s in each of Bessell-*B*, *V*, *R*, & CTIO-*I* filters over the *Chandra* field.

We processed the images using standard IRAF tasks, and calibrated the astrometry using the 2MASS catalogue as a reference. The astrometric residuals on each CCD frame were $\sim 0.2''$. We reprojected and stacked the images using the SWARP[7] utility. All frames were normalized to ADU/second units and combined using weight-maps constructed from flat-fields and bad pixel masks. The initial source search and photometry were performed on the stacked images using SExtractor (Bertin & Arnouts 1996).

After boresighting the initial IMACS source list to the *Chandra* sources (Zhao et al. 2005), and applying offsets of ΔRA = 0.088(51)$''$, ΔDEC = 0.498(50)$''$ to the X-ray coordinates, we found a potential counterpart in the *B* and *V* band images within the search area of the *Chandra* source. In Fig. 5a, the source search area is marked by the (red) circle, the radius of which is the 2σ quadratic sum of the boresight error and the positional errors of the X-ray and optical sources (Zhao et al. 2005). The potential counterpart (indicated with green tick marks in the figure) is not completely resolved with

[7] http://terapix.iap.fr

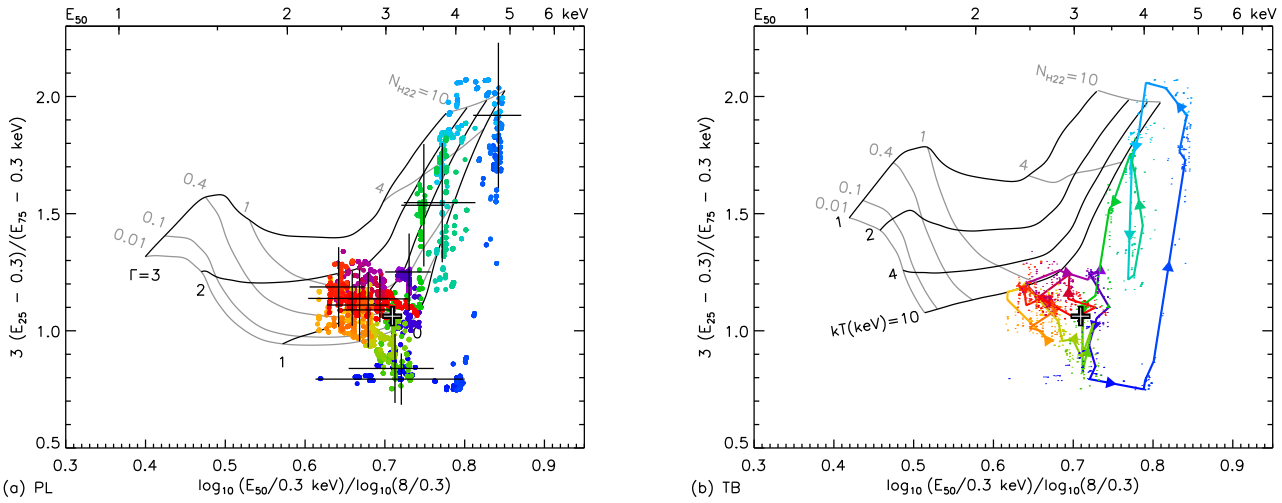

FIG. 4.— The quantile diagram of CXOPS J180354.3-300005 as a function of modulation phase, color-coded to match the phase in Fig. 3b (see the electronic version). Both panels show the same data and the 10 binned data points are shown in (a). The grid in (a) is for simple power law models with Γ = 0, 1, 2 & 3 and $N_{\rm H22}$ = 0.01, 0.1, 0.4 , 1, 4 & 10 and in (b) for thermal Bremsstrahlung model with kT = 1, 2, 4, 10 keV and the same $N_{\rm H22}$. The arrows in (b) show the temporal orientation of the spectral change. There is a strong correlation between the quantiles and the modulation phase. The energy quantile E_x corresponds to the energy below which x% of the counts are detected in the 0.3–8.0 keV band. The top-axis of the quantile diagram is labeled by the median energy (E_{50}).

a nearby star (orange). Therefore, we generate a PSF model using a few bright isolated sources within $\sim 30''$, and perform PSF fitting to the two sources in the B band image (where the candidate counterpart is brightest and its neighbor is faintest) using the DAOPHOT package ALLSTAR in IRAF in order to derive the position and magnitude of the source. The position of the optical source is (RA, DEC) J2000 = (18:03:54.45, –30:00:06.3). For the V, I and R band images, we performed PSF fitting with the fixed positions given by the results of the PSF fitting in the B band image. The instrumental B, V and I magnitudes are calibrated against OGLE-II (Udalski 2002) stars in the field by first order polynomial fits.

Fig. 5b shows a calibrated color-magnitude diagram (CMD) for stars within $\sim 30''$ of the potential counterpart (green diamond) and the neighbor (orange square). The CMD shows the potential counterpart is bluer than the majority of field stars. The calibrated apparent magnitude of the optical counterpart is B = 22.2(1), V = 21.7(1) and I = 20.6(1) where the errors are the output of the DAOPHOT. Taking the interstellar extinction to BW to be A_V = 0–1.4, $E(B-V)$ = 0–0.45 leads to a de-reddened color index $(B-V)_0$ = 0.05–0.5 for the optical counterpart. This value is in the typical range for cataclysmic variables, see for example Allen (1977), table 17.9. The number of blue sources (24 sources with $B-V < 0.7$) falling in the error circle by chance is about 0.03.

We estimate the ratio of the unabsorbed X-ray to optical flux, $\log(F_X/F_V)$ = 0.63–1.12 for A_V = 0.0–1.4, where F_X is in the 2–8 keV range. The blue color of the optical source and the relatively high value of $\log(F_X/F_V)$ (typically < -2.5 for normal stars) are consistent with the accretion nature of the X-ray emission from the source, indicating that the optical source is a good candidate for being the counterpart.

5. DISCUSSION

The lack of a bright optical counterpart ($V \lesssim 14$) rules out a high mass X-ray binary (HMXB) and hence a neutron star pulsar for the system. The relatively hard spectrum rules out a quiescent low mass X-ray binary or a coronal nature of the X-ray emission. In fact, the X-ray properties of the source show classic signatures of IPs such as the intrinsically hard X-ray spectrum with, although marginal, a possible iron emission line and the X-ray pulsation correlated with the internal absorption at a period of 1028 s. The estimated luminosity of the system (see below) is also consistent with IPs. A likely scenario for modulating internal absorption at the spin period is that in a bright phase we have a relatively uninterrupted view of the emission region on the surface of the WD whereas in a faint phase we are looking at the emission region through the channelled accretion stream, which attenuates the X-rays.

In the following, we estimate the likely distance of the source to see if the system could belong to the GB population, the majority of which are believed to be IPs. If we assume a typical range of absolute V magnitude for a CV (M_V $\sim$ 5.5–10.5) (Patterson 1998) and the known reddening in the region (A_V = 1.4 at > 3 kpc) (Marshall et al. 2006), the source distance should be in the range of 2–10 kpc for $V \sim 22$, suggesting that the source is non-local. Note if this optical source is not the counterpart of the X-ray source ($V \gtrsim 22$), the distance estimate becomes the lower bound, which reinforces the argument that the X-ray source is non-local. The corresponding average X-ray luminosity would be $6\times10^{31}-10^{33}$ ergs s^{-1} in the 2–8 keV range. According to the population synthesis model for the magnetic CVs in the GC region by Ruiter et al. (2006); Heinke et al. (2008), this luminosity range is acceptable for non-degenerate magnetic CVs.

We can take this a step further. Assuming the space density of IPs follows the stellar density, in BW we expect IPs are more likely found in the GB at a distance of 6–10 kpc. For instance, if we use the stellar model (model A) in Hong et al. (2009), shown as (red) squares in Fig. 6, the probability that a given IP in the field is at 6–10 kpc is about 80% when there is no luminosity constraint. We can convert the luminosity distribution of IPs in Ruiter et al. (2006) (their standard model) to a probable distance distribution for the given flux of the source (1.2×10^{-13} ergs cm^{-2} s^{-1} in 2–8 keV), which is shown as (blue) diamonds in Fig. 6. Now if we combine these two distance-dependent constraints, we can estimate the probability distribution of the source distance for the given X-ray flux (black circles). The result indicates there is about a 70% chance that the source is at a distance of 6–10 kpc among

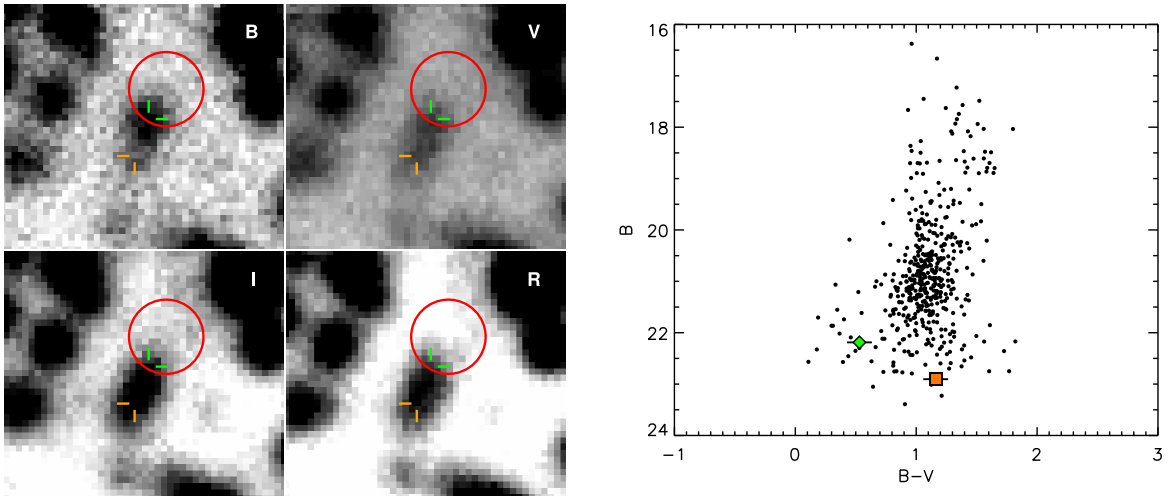

FIG. 5.— The finding chart in the B, V, I and R band images (left) and the color-magnitude diagram (CMD) in B vs. $B-V$ (right). In the finding chart the (red) circle centered at the X-ray source (radius: 2σ of the composite errors, $0.66''$) indicates the search region for counterparts. The candidate counterpart and the neighbor star are marked by green and orange tick marks respectively. The CMD compares the two marked sources with the field stars within $30''$. The potential counterpart (green diamond) is mildly bluer than the most field stars.

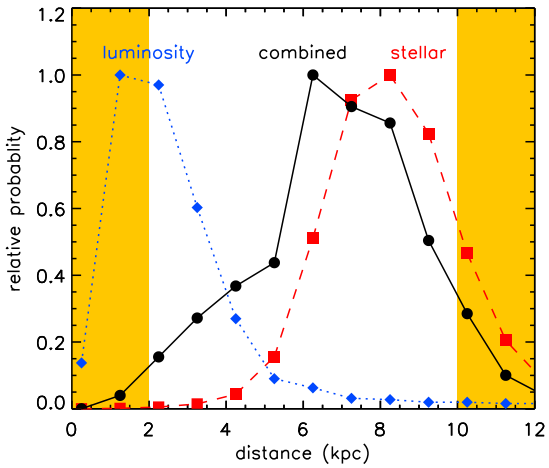

FIG. 6.— The combined probability distribution of the source distance (black circles) from the stellar distribution (red squares, model A in Hong et al. (2009)) and the distance distribution based on the X-ray luminosity (blue diamonds, the standard model in Ruiter et al. (2006)) for the given flux of the source (1.2×10^{-13} ergs cm^{-2} s^{-1}). The unshaded region represents the acceptable distance for the source based on the V magnitude of the potential counterpart. Each distribution is rebinned in 0.5 kpc intervals.

the possible range of 2–10 kpc set by the V magnitude of the potential counterpart (64% chance without any constraint from the potential counterpart). This estimate mildly favors the source being a bright IP in the GB X-ray population rather than an IP outside of the GB. Note there are large uncertainties in the assumptions of this estimate. For instance, the statistics in the model of the X-ray luminosity distribution at $> 10^{32}$ ergs s^{-1} is relatively poor (see Fig. 1 in Ruiter et al. (2006)).

If indeed there are numerous IPs among the hard X-ray sources found in this region, long term X-ray monitoring can lead to a direct identification of many sources through detection of pulsations. For instance, for a 1 Ms exposure of the BW, we expect to detect > 500 counts from IPs with 10^{32} ergs s^{-1} in the GB at 8 kpc, which allows for a direct detection of modulations if present. A crude scaling using $N(>S) \sim S^{-1.5}$ predicts we should be able to identify ~ 30 sources or more in BW from such an exposure, and at 10^{32} ergs s^{-1} or below, we start to see the major part of the luminosity distribution of the magnetic CVs according to Ruiter et al. (2006); Heinke et al. (2008). In addition, low extinction regions such as the Window fields are better suited for this approach than high extinction fields such as Sgr A* since the dust in the high extinction fields would attenuate the apparent X-ray modulation or spectral changes dramatically, which would make the pulsation very hard to detect. For example, the spectral variation seen in Fig. 4 would not have been easily identifiable with the substantial external extinction ($N_{\rm H22} \sim 6$, a nominal value for the GC (Baganoff et al. 2003)) if the source was located in the GC in the Sgr A* field.

We thank A. Ruiter for providing the X-ray luminosity distribution of IPs. This work is supported in part by NASA/*Chandra* grants GO6-7088X, GO7-8090X and GO8-9093X.

REFERENCES

Allen, K. W., 1977, Astrophysical quantities., 3rd Ed., Moskva: Mir.
Baganoff, F. K. et al. 2003, ApJ, 591, 891.
Bertin, E. & Arnouts, S., 1996, ApJ, 117, 393.
Cleveland, W. S., 1994, The Elements of Graphing Data, Hobart Press, 2nd edition.
Drimmel, R., Cabrera-Lavers, A., & Lopez-Corredoira, M., 2003, ApJ, 409, 205.
Grindlay, J.E. et al. 2005, ApJ, 635, 907
Grindlay, J.E. et al. 2009, in preparation.
Freeman, P.E. et al. 2002, ApJS, 138, 185.
Gehrels, N. et al. 1986, ApJ, 303, 336.
Heinke, C. O., et al., 2008 AIPC, 1010, 136.
Hong, J, Schlegel, E. M. & Grindlay, J. E., 2004, ApJ, 614, 508. (H04)
Hong, J, et al. 2005, ApJ, 635, 907. (H05)
Hong, J, et al. 2009, submitted to ApJ.
Hong, J, et al. 2009b, in preparation.
Laycock, S. et al. 2005, ApJL, 634, 53 (L05)
Marshall, D. J. et al. 2006, A&A, 453, 635
Muno, M. P. et al. 2003, ApJ, 589, 225 (M03)
Muno, M. P. et al. 2003a, ApJ, 589, 225
Muno, M. P. et al. 2003b, ApJ, 599, 465
Muno, M. P. et al. 2004, ApJ, 613, 1179 (M04)

Norton, A. J., Wynn, G. A. & Somerscales, R. V., 2004 ApJ, 614, 349
Patterson, J., 1998, PASJ, 110, 1132.
Predehl, P. & Schmitt, J. H. M. M., 1995, A&A, 293, 889.
Ramsay, M. & Cropper, M. 2004, MNRAS, 347, 497.
Ritter, H. & Kolb, U., 2003, ApJ, 404, 301
Ruiter, A., Belczynski, K. & Harrison, T. 2006, ApJL, 640, 167.
Scargle, J. D., 1982, ApJ, 263, 835.
Schlegel, D., Finkbeiner, D. & Davis, M., 1998, ApJ, 500, 525.
Sumi, T., 2004, MNRAS, 349, 193.
Udalski, T., 2002, ACTA Astronomica, 52, 217.
Wang, Q. D. , Gotthelf, E. V. & Lang, C. C., 2002, Nature, 415, 148.
van den Berg, M. et al. 2006, ApJL, 135, 647
van den Berg, M. et al. 2009, submitted to ApJ.
Zhao, P. et al. 2005, ApJS, 161, 429.